Journal of Low Temperature Physics (2022) 209:1119–1127
https://doi.org/10.1007/s10909-022-02739-3

Numerical Calculation of the Thermodynamic Properties of Silver Erbium Alloys for Use in Metallic Magnetic Calorimeters

Matthew Herbst[1] · Arnulf Barth[1] · Andreas Fleischmann[1] · Loredana Gastaldo[1] · Daniel Hengstler[1] · Neven Kovac[1] · Federica Mantegazzini[1] · Andreas Reifenberger[1] · Christian Enss[1]

Received: 1 November 2021 / Accepted: 21 April 2022 / Published online: 14 May 2022

Abstract
Using dilute silver erbium alloys as a paramagnetic temperature sensor in metallic magnetic calorimeters (MMCs) has the advantage of the host material not having a nuclear quadrupole moment, in contrast to the alternative of using gold erbium alloys. We present numerical calculations of the specific heat and magnetization of Ag:Er, which are necessary for designing and optimizing MMCs using this type of alloy as sensor material. The parameter ranges we consider are temperatures between 1 mK and 1 K, external magnetic fields of up to 20 mT, and erbium concentrations of up to 2000 ppm. The system is dominated by an interplay of crystal field effects, Zeeman splitting, and the RKKY interaction between erbium ions, with certain specific constellations of erbium ions having noticeable effects on the specific heat. Increasing the external magnetic field or assuming a decreased strength of the RKKY interaction leads to a higher magnetization and a narrowing of the main Schottky peak, while changes in the erbium concentration can be well described by parameter scaling.

Keywords Heat capacity · Schottky anomaly · RKKY interaction · Dilute erbium alloys · Metallic magnetic calorimeters

1 Introduction

Metallic Magnetic Calorimeters (MMCs) are cryogenic particle detectors that rely on reading out the temperature-dependent magnetization of a paramagnetic sensor material in order to transform the temperature increase caused by a particle

✉ Matthew Herbst
matthew.herbst@kip.uni-heidelberg.de

[1] Kirchhoff Institute for Physics, Heidelberg University, Heidelberg, Germany

impacting the detector into a measurable signal [1]. Dilute alloys of erbium and noble metals placed in a weak magnetic field are well suited to be such a sensor material [2], due to the small de Gennes factor [3] of Er^{3+}, and the fast electron-spin relaxation time allowing for short signal rise times [4] of under 100 ns[5]. Initially, gold was most commonly used as a host [6–8], as the low RKKY interaction in gold results in a larger magnetic response. A number of detailed analyses of Au:Er are available [9, 10], including the full quantum mechanical simulations by Schönefeld [11, 12], which match experimental data well. However, it was also observed that the nuclear magnetic moment $I = 3/2$ of the ^{197}Au nucleus can cause an additional heat capacity when the nuclear levels are split by a nearby erbium ion breaking the cubic symmetry of the electric field gradient at this lattice site [12]. The interaction of the nuclear quadrupole moment with the electric field gradient leads to an additional heat capacity and a more complex pulse shape at low temperatures, making data evaluation difficult. One solution is using silver as a host material, where this feature is not observed [13], since silver does not have a nuclear quadrupole moment. Experimentalists must weigh this advantage against the disadvantage of the RKKY interaction in silver being roughly 2–3 times stronger than in gold [14, 15], which decreases the magnetic response of the sensor. In recent years, MMCs operating at the lowest temperatures have increasingly used Ag:Er sensors [16–19].

One main advantage of MMCs is that they operate near thermal equilibrium. Additionally, the signal size they produce depends only on geometrical factors and on bulk thermodynamic properties, such as the specific heat and magnetization. As a result, accurate simulations of an MMCs inherent noise and energy resolution, such as described by Fleischmann et al. [20], are possible when given the specific heat and magnetization of the sensor material as input parameters. In this article, we present simulations tailored to meet this need, as well as more detailed analyses of Ag:Er regarding the influence of external magnetic fields, the strength of the RKKY interaction, and the erbium concentration.

2 Simulation of Interactions in Ag:Er

For our applications, the atomic concentration x_{Er} of erbium in the sensor material is no larger than a few thousand ppm. The resulting alloy is a solid solution [21], with the erbium taking the place of silver atoms in the fcc lattice. The erbium loses three electrons to the conduction band, resulting in Er^{3+} ions with quantum numbers $L = 6$, $S = 3/2$, $J = 15/2$, and Landé factor $g_{\mathrm{J}} = 6/5$. However, the crystal field of the silver causes an energy splitting of the 16-fold degenerate $J = 15/2$ ground state into a number of multiplets. The lowest of these is a Γ_7 doublet, which is separated by a $25\,\mathrm{K} \cdot k_{\mathrm{B}}$ gap to the next lowest multiplet [22]. For our application of MMCs operated at temperatures below 1K, this allows us to reduce the system to this lowest doublet state, with an effective spin $S = 1/2$ and an effective Landé factor of $\tilde{g} = 6.8$ [23]. The external magnetic field $\boldsymbol{B}$ then splits the Γ_7 doublet, which we describe via the Zeeman Hamiltonian

$$H_{\text{Zeeman}} = -\boldsymbol{\mu} \cdot \boldsymbol{B} = -\tilde{g}\mu_{\text{B}} \boldsymbol{S} \cdot \boldsymbol{B} \quad . \tag{1}$$

Here, $\boldsymbol{\mu}$ and $\boldsymbol{S}$ are the magnetic moment and spin of an erbium ion and μ_{B} is the Bohr magneton. The result of such an energy splitting of $\Delta E = \tilde{g}\mu_{\text{B}} B$ is a Schottky anomaly in the specific heat with a maximum at $T_{\text{max}} \approx 0.42\, \Delta E\, k_{\text{B}}^{-1} \approx 10\,\text{mK}$ for a typical magnetic field of $B = 5\,\text{mT}$. The magnetization follows a Curie-like $1/T$ law and saturates at low temperatures. Note that we disregard hyperfine splitting, as we assume that isotopically enriched ^{168}Er is used, which has no nuclear spin.

In a further step, consider two erbium ions with spins $\boldsymbol{S}_i$ and $\boldsymbol{S}_j$ at a distance r_{ij} from each other. They interact via the magnetic dipole–dipole interaction

$$H_{ij}^{\text{dipole}} = \Gamma_{\text{dipole}} \frac{1}{(2k_{\text{F}} r_{ij})^3} \left[\boldsymbol{S}_i \cdot \boldsymbol{S}_j - 3\left(\boldsymbol{S}_i \cdot \hat{\boldsymbol{r}}_{ij}\right)\left(\boldsymbol{S}_j \cdot \hat{\boldsymbol{r}}_{ij}\right) \right] \quad , \tag{2}$$

where we have artificially introduced the Fermi wave vector $k_{\text{F}} = 1.2 \cdot 10^{10}\,\text{m}^{-1}$ of the conduction electrons of the silver, and via the RKKY interaction

$$H_{ij}^{\text{RKKY}} = \Gamma_{\text{RKKY}} \left(\boldsymbol{S}_i \cdot \boldsymbol{S}_j\right) F(2k_{\text{F}} r_{ij}) \quad \text{with} \quad F(\rho) = \rho^{-3} \left(\cos\rho - \frac{\sin\rho}{\rho} \right) \quad . \tag{3}$$

We have introduced the normalized vector $\hat{\boldsymbol{r}}_{ij}$ in direction $\boldsymbol{r}_i - \boldsymbol{r}_j$, and the two prefactors

$$\Gamma_{\text{dipole}} = \frac{\mu_0}{4\pi} \left(\tilde{g}\mu_{\text{B}}\right)^2 \left(2k_{\text{F}}\right)^3 \quad \text{and} \quad \Gamma_{\text{RKKY}} = \mathfrak{J}^2 \frac{4V_0^2 m_{\text{e}}^* k_{\text{F}}^4}{\hbar^2 (2\pi)^3} \frac{\tilde{g}^2 (g_{\text{J}} - 1)^2}{g_{\text{J}}^2} \quad , \tag{4}$$

with the vacuum permeability μ_0, the coupling energy $\mathfrak{J}$ between the localized spins and the conduction electrons, the volume V_0 of the elementary cell, and the effective mass m_{e}^* of the conduction electrons of the silver. An important metric is the relative strength $\alpha = \Gamma_{\text{RKKY}}/\Gamma_{\text{dipole}}$ of the two interactions. For Ag:Er, α is not precisely known, with ESR measurements placing it between 6.4 and 13.7 [14], and magnetization measurements using MMCs suggesting $\alpha = 12.5$ and $\alpha = 15$ [15, 24]. In general, however, we assume the RKKY interaction to be more significant than dipole–dipole interactions.

In order to simulate the thermodynamic properties of Ag:Er alloys, we follow an approach similar to the one first described for Au:Er alloys by Schönefeld [11, 12]. In our model, we construct a cubic section of an fcc lattice and randomly distribute $N_{\text{Er}} = 9$ erbium ions on the lattice sites. Increasing the number of erbium ions beyond nine does not affect our results significantly, while dramatically increasing computation time. Note, however, that spin glass effects, which we expect to occur in the low mK range [9, 25], are not the focus here and are described poorly. The volume V of the fcc cube is determined by the desired erbium concentration. As erbium ions near the boundary of the cube would experience a lower effective erbium concentration, we copy the cube 26 times to form a 3×3×3 grid of identical lattice sections. A random direction is chosen for the external magnetic field B. Based on this model, we construct the Hamiltonian of the system via Eqs. 1, 2, and 3. From the resulting eigenvalues E_i we calculate the partition function

$$Z = \sum_i z_i = \sum_i e^{-\frac{E_i}{k_B T}} \tag{5}$$

and the occupation probability $p_i = z_i/Z$ for each eigenstate. The heat capacity C and magnetization M of the system follow via

$$C = \frac{1}{k_B T^2}\left(\langle E^2\rangle - \langle E\rangle^2\right) \quad \text{and} \quad M = -\frac{1}{V}\left\langle \frac{\partial E}{\partial B}\right\rangle \quad , \tag{6}$$

where the angular brackets denote the expectation value $\langle X\rangle = \sum X_i p_i$ of a variable X. By repeating these steps 10,000 times with random distributions of erbium ions and averaging over the resulting physical quantities, we achieve consistent and representative results. As a final step, the heat capacity of the electronic and phononic contribution of the silver is added. Silver's diamagnetic contribution to the magnetization can be neglected.

The results of a simulation with $x_{\mathrm{Er}} = 500\,\mathrm{ppm}$, $B = 5\,\mathrm{mT}$, and $\alpha = 15$ appear in Fig. 1, with the specific heat c per mole of Ag:Er on the left and the magnetization M on the right. We plot a set of 300 randomly chosen individual simulations in green, to which the contribution of the silver has already been added. The average over the entire set of 10,000 simulations appears in black. The main feature in the specific heat curve is the Schottky peak from the Zeeman splitting of the Γ_7 doublet. Without any other interaction, this would result in the blue curve. However, the interactions between erbium ions cause shifts of the energy levels, which are dependent on the random distances r_{ij} between erbium ions. As a result, the averaged peak is broader, and due to conservation of the entropy $S = \int C(T)/T\,\mathrm{d}T$, necessarily less tall than the Schottky peak in a pure Zeeman system.

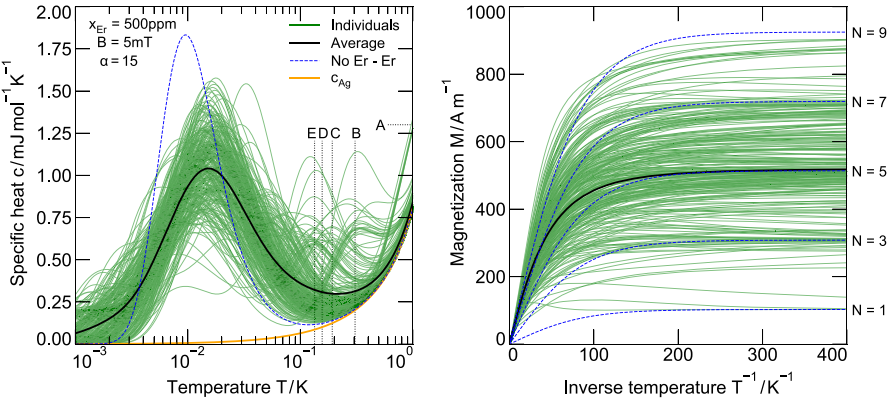

Fig. 1 Result of a simulation of Ag:Er with $x_{\mathrm{Er}} = 500\,\mathrm{ppm}$, $B = 5\,\mathrm{mT}$, and $\alpha = 15$. The calculated specific heat per mole of Ag:Er (*left*) and the magnetization (*right*) of 300 of the 10,000 simulated systems appear in *green*, together with the averaged curve in *black*. Respective curves for a non-interacting system appear in *blue*, with N representing the number of free magnetic moments. The electronic and phononic contribution of the silver host material appears in *orange*. Expected Schottky peaks for certain erbium constellations are marked with *letters*, see Table 1 (Color figure online.)

In a number of individual systems we see secondary peaks, most notably at higher temperatures. These are present in systems where a particular pair of erbium ions happens to have a strong RKKY interaction. In order to assign each of these secondary peaks a certain distribution of erbium ions, consider a simple system with two erbium ions interacting only via the RKKY interaction. All possible relative positions of the two erbium ions that result in a Schottky anomaly with $T_{\max} > 100\,\mathrm{mK}$ are listed in Table 1, with the relative positions and resulting distances r_{ij} in units of the cubic lattice constant $a = 4.1$ Å. For each possible separation, we list only one of the N_{perm} possible x,y, and z offsets. The calculated $T_{\max}$ are marked in Fig. 1 and we see a good match to the side maxima of the full simulation, with small deviations due to other interactions. Note that the number of individual systems that feature one of the listed Schottky anomalies correlates with N_{perm}, resulting in peaks B and E being more prominent than peaks C and D. In the temperature range of $80\,\mathrm{mK} - 500\,\mathrm{mK}$, the averaged specific heat (black) is strongly affected by the relatively small number of systems with a side peak and lies noticeably above the specific heat of most of the individual systems without a side peak.

We consider now the magnetization, plotted on the right-hand side of Fig. 1 as a function of the inverse temperature. In the limit of non-interacting spins, the magnetization is described by the Brillouin function

$$M = \frac{N}{V}\tilde{g}S\mu_{\mathrm{B}}\left[\frac{2S+1}{2S}\coth\left(\frac{(2S+1)h}{2S}\right) - \frac{1}{2S}\coth\left(\frac{h}{2S}\right)\right] \quad , \tag{7}$$

with the number N of free spins, the volume V of the simulated lattice section, and $h = \tilde{g}S\mu_{\mathrm{B}}B/(k_{\mathrm{B}}T)$. This function appears in blue in Fig. 1 for $N = 1, 3, 5, 7$, and 9, where it describes clusters of individual systems well. If two of the original $N_{\mathrm{Er}} = 9$ erbium ions are so close that they are locked in an anti-parallel orientation, they can no longer contribute to the magnetization and the system is effectively reduced to $N_{\mathrm{Er}} - 2 = 7$ spins. For erbium distributions with multiple such pairs, the number of free erbium ions is reduced further to 5, 3, or 1 free spin. We thus observe a

Table 1 Locations of the Schottky anomalies in a system of two erbium ions interacting only via RKKY for $\alpha = 15$

$\Delta x/a$	$\Delta y/a$	$\Delta z/a$	r_{ij}/a	N_{perm}	$T_{\max}$/mK	Fig. 1 mark
0	0.5	0.5	0.71	12	4467	–
0.5	0.5	1	1.22	24	1082	A
0.5	1	1.5	1.87	48	306	B
0	0	2	2	6	192	C
0	1	1	1.41	12	156	D
0	0.5	2.5	2.55	72	134	E

The first three columns denote one example for the relative x, y, and z positions in the fcc lattice in units of the cubic lattice constant $a = 4.1$ Å. Column 4 lists the resulting distance r_{ij}. The number of possible permutations N_{perm} gives a measure for the probability of a system fulfilling that characteristic distance requirement. Entries are sorted by the expected locations $T_{\max}$ of the resulting Schottky anomaly, which are marked in Fig. 1

distinct division into plateaus at low temperatures. Averaging these curves (black) then results in an accurate representation of the material.

3 Influence of B, α, and x_{Er}

Based on the system introduced in Fig. 1 with $B = 5\,\mathrm{mT}$, $\alpha = 15$, and $x_{\mathrm{Er}} = 500\,\mathrm{ppm}$, we analyze the effects these parameters have on our simulations.

The specific heat of five systems in different magnetic fields appears in the top left of Fig. 2. Following the calculations in Sect. 2, the location of the Schottky anomaly of the unperturbed system (dashed lines) is proportional to B. In the limit of large magnetic fields, the interacting system (solid lines) approaches this

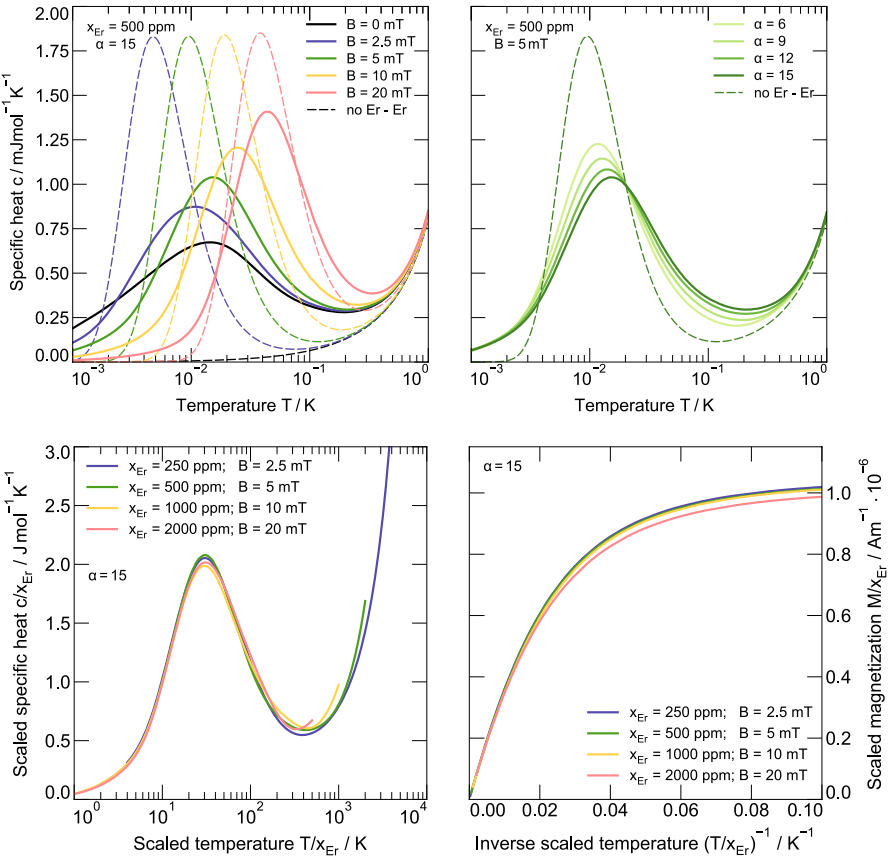

Fig. 2 Analysis of a Ag:Er system when varying different parameters. The specific heat is plotted for different magnetic fields (*top left*) and for different α (*top right*). The specific heat and magnetization scaled with erbium concentration plotted against a scaled temperature axis demonstrates the scaling law (*bottom*). Comparable simulations with $\alpha = 5$, 10, and 12.5 are available online. The system presented in Fig. 1 with $x_{\mathrm{Er}} = 500\,\mathrm{ppm}$, $B = 5\,\mathrm{mT}$, and $\alpha = 15$ appears in *dark green* in all plots (Color figure online.)

Zeeman-Schottky limit, since the influence of the magnetic field overshadows erbium-erbium interactions. For low magnetic fields, the RKKY interaction is dominant, with a number of characteristic peaks overlapping as in Fig. 1, leading to a broad maximum in the specific heat. The precise location and shape of this peak are dependent on α and the erbium concentration.

An analysis of the effect that $\alpha = \Gamma_{\mathrm{RKKY}}/\Gamma_{\mathrm{dipole}}$ has on the specific heat of Ag:Er appears on the top right of Fig. 2. As the precise value of α is unknown, the simulations cover the entire range of suggested values from $\alpha = 6$ to $\alpha = 15$ [14, 15, 24]. A larger α, and thus a stronger RKKY interaction, leads to a broadening and flattening of the Schottky peak, similar to the effect a decreased magnetic field has on the system. However, T_{max} is shifted towards higher temperatures, since the stronger forces between erbium ions lead to larger energy gaps between eigenstates. The lower specific heat in the temperature range below 20 mK, where MMCs are typically operated, seems to favor systems with a large α. This is, however, offset by a reduction in $\mathrm{d}M/\mathrm{d}T$ (not pictured) caused by an increased number of erbium ions being locked through RKKY interactions. In an analysis of individual simulations as presented in Fig. 1 (right), more systems were described by a lower N than in a comparable simulation with a reduced α.

Regarding the erbium concentration x_{Er}, we expect the scaling law outlined by Souletie et al. [26] to hold. That is, a change in x_{Er} is equivalent to scaling the other physical quantities:

$$x_{\mathrm{Er}} \to x'_{\mathrm{Er}} \quad \Leftrightarrow \quad \begin{aligned} T &\to T' &&= T &&\cdot\, x_{\mathrm{Er}}/x'_{\mathrm{Er}} \\ B &\to B' &&= B &&\cdot\, x_{\mathrm{Er}}/x'_{\mathrm{Er}} \\ c(T,B) &\to c'(T',B') &&= c(T,B) &&\cdot\, x_{\mathrm{Er}}/x'_{\mathrm{Er}} \\ M(T,B) &\to M'(T',B') &&= M(T,B) &&\cdot\, x_{\mathrm{Er}}/x'_{\mathrm{Er}} \end{aligned} \tag{8}$$

Conversely, when scaling all quantities equally, curves should stay identical. Four different systems with $\alpha = 15$ and equal ratio B/x_{Er} appear on the bottom of Fig. 2 with appropriately scaled axes ($\alpha = 5$, 10, and 12.5 are available online). The scaled specific heat is almost identical between all systems, with even the contribution of the conduction electrons not disturbing the scaling, which was derived for the spin contribution only. Only the phononic contribution of the silver is not described by the scaling law, which leads to discrepancies at high temperatures. Considering the magnetization, we see a small deviation for simulations with the highest erbium concentrations. In these cases, the average distance between erbium ions is so low that we can no longer fully ignore the oscillatory nature of the RKKY interaction. Peaks in the RKKY interaction lead to an increased freezing of the spins in certain eigenstates, reducing the available spins which can be oriented with respect to $\boldsymbol{B}$. This results in a lower magnetization. We conclude that for concentrations of $x_{\mathrm{Er}} \lesssim 1000$ ppm, the scaling law is a good approximation, if one calculates the specific heat contribution of the lattice separately.

Acknowledgements Part of this research was performed in the framework of the DFG Research Unit FOR2202 "Neutrino Mass Determination by Electron Capture in 163Ho, ECHo" (funding under EN 299/7-1 and EN 299/7-2, EN 299/8-1, GA 2219/2-1 and GA 2219/2-2). The research leading to these results has received funding from the European Union's Horizon 2020 Research and Innovation

Programme, under Grant Agreement no 824109 (European Microkelvin Platform). A. Barth and F. Mantegazzini acknowledge support by the Research Training Group HighRR (GRK 2058) funded through the Deutsche Forschungsgemeinschaft, DFG.

Funding Open Access funding enabled and organized by Projekt DEAL.

Data Availability The datasets generated during and/or analyzed during the current study, including additional simulations demonstrating the scaling law for $\alpha = 5$, 10, and 12.5, are available in the Zenodo repository, https://doi.org/10.5281/zenodo.5637329.

Declarations

Conflict of interest The authors declare that they have no conflict of interest.

References

1. A. Fleischmann, C. Enss, G.M. Seidel, in *Cryogenic Particle Detection*, ed. by C. Enss (Springer, Berlin, 2005), p. 151. https://doi.org/10.1007/10933596_4
2. S.R. Bandler, C. Enss, R.E. Lanou, H.J. Maris, T. More, F.S. Porter, G.M. Seidel, J. Low Temp. Phys. **93**, 709 (1993). https://doi.org/10.1007/BF00693500
3. P.G. de Gennes, Comp. Rend. Acad. Sci. **247**, 1836 (1958)
4. M.E. Sjöstrand, G. Seidel, Phys. Rev. B **11**, 3292 (1975). https://doi.org/10.1103/PhysRevB.11.3292
5. H. Rotzinger, J. Adams, S.R. Bandler, J. Beyer, H. Eguchi, E. Figueroa-Feliciano, W. Hsieh, G.M. Seidel, T. Stevenson, J. Low Temp. Phys. **151**, 351 (2008). https://doi.org/10.1007/s10909-007-9658-5
6. W.T. Hsieh, J.A. Adams, S.R. Bandler, J. Beyer, K.L. Denis, H. Eguchi, E. Figueroa-Feliciano, H. Rotzinger, G.H. Schneider, G.M. Seidel, T.R. Stevenson, D.E. Travers, J. Low Temp. Phys. **151**, 357 (2008). https://doi.org/10.1007/s10909-007-9661-x
7. M. Rodrigues, A. Pabinger, S. Lausberg, M. Loidl, B. Censier, J. Bouchard, L. Fleischmann, A. Fleischmann, C. Enss, AIP Conf. Proc. **1185**, 583 (2009). https://doi.org/10.1063/1.3292409
8. L. Fleischmann, M. Linck, A. Burck, C. Domesle, S. Kempf, A. Pabinger, C. Pies, J.P. Porst, H. Rotzinger, S. Schafer, R. Weldle, A. Fleischmann, C. Enss, G.M. Seidel, IEEE Trans. Appl. Supercond. **19**, 63 (2009). https://doi.org/10.1109/TASC.2009.2012724
9. T. Herrmannsdörfer, R. König, C. Enss, Physica B **284–288**, 1698 (2000). https://doi.org/10.1016/S0921-4526(99)02942-7
10. B.L. Zink, K.D. Irwin, G.C. Hilton, J.N. Ullom, D.P. Pappas, J. Appl. Phys. **99**, 08B303 (2006). https://doi.org/10.1063/1.2159207
11. J. Schönefeld, Entwicklung eines mikrostrukturierten magnetischen Tieftemperatur-Kalorimeters zum hochauflösenden Nachweis von einzelnen Röntgenquanten. Ph.D. thesis, Heidelberg University (2000)
12. C. Enss, A. Fleischmann, K. Horst, J. Schönefeld, J. Sollner, J.S. Adams, Y.H. Huang, Y.H. Kim, G.M. Seidel, J. Low Temp. Phys. **121**, 137 (2000). https://doi.org/10.1023/A:1004863823166

13. C. Enss, A. Fleischmann, T. Görlach, Y.H. Kim, G.M. Seidel, H.F. Braun, AIP Conf. Proc. **605**, 71 (2002). https://doi.org/10.1063/1.1457598
14. L.J. Tao, D. Davidov, R. Orbach, E.P. Chock, Phys. Rev. B **4**, 5 (1971). https://doi.org/10.1103/PhysRevB.4.5
15. D. Hengstler, Development and characterization of two-dimensional metallic magnetic calorimeter arrays for the high-resolution X-ray spectroscopy. Ph.D. thesis, Heidelberg University (2017). https://doi.org/10.11588/heidok.00023815
16. S.T.P. Boyd, R. Hummatov, G.B. Kim, L.N. Le, J.A. Hall, R. Cantor, S. Friedrich, J. Low Temp. Phys. **193**, 435 (2018). https://doi.org/10.1007/s10909-018-2017-x
17. A. Reifenberger, A. Reiser, S. Kempf, A. Fleischmann, C. Enss, Rev. Sci. Instrum. **91**, 035118 (2020). https://doi.org/10.1063/1.5139090
18. T. Sikorsky, J. Geist, D. Hengstler, S. Kempf, L. Gastaldo, C. Enss, C. Mokry, J. Runke, C.E. Düllmann, P. Wobrauschek, K. Beeks, V. Rosecker, J.H. Sterba, G. Kazakov, T. Schumm, A. Fleischmann, Phys. Rev. Lett. **125**, 142503 (2020). https://doi.org/10.1103/PhysRevLett.125.142503
19. S.G. Kim, J.A. Jeon, H.B. Kim, H.L. Kim, S.R. Kim, Y.H. Kim, D.H. Kwon, M.K. Lee, Y.C. Lee, K.R. Woo, IEEE Trans. Appl. Supercond. **31**, 1 (2021). https://doi.org/10.1109/TASC.2021.3066179
20. A. Fleischmann, L. Gastaldo, S. Kempf, A. Kirsch, A. Pabinger, C. Pies, J. P. Porst, P. Ranitzsch, S. Schäfer, F. v Seggern, T. Wolf, C. Enss, G. M. Seidel, AIP Conf. Proc. **571**, 1185 (2009). https://doi.org/10.1063/1.3292407
21. K.A. Gschneidner, F.W. Calderwood, Bull. Alloy Phase Diagr. **6**, 17 (1985). https://doi.org/10.1007/BF02871168
22. W. Hahn, M. Loewenhaupt, B. Frick, Physica B **180–181**, 176 (1992). https://doi.org/10.1016/0921-4526(92)90698-R
23. A. Abragam, B. Bleaney, *Electron Paramagnetic Resonance of Transition Ions* (Clarendon Press, Oxford, 1970)
24. A. Burck, Entwicklung großflächiger mikrostrukturierter magnetischer Kalorimeter mit Au:Er- und Ag:Er-Sensoren für den energieaufgelösten Nachweis von Röntgenquanten und hochenergetischen Teilchen. Ph.D. thesis, Heidelberg University (2008). https://doi.org/10.11588/heidok.00008832
25. A. Fleischmann, J. Schönefeld, J. Sollner, C. Enss, J.S. Adams, S.R. Bandler, Y.H. Kim, G.M. Seidel, J. Low Temp. Phys. **118**, 7 (2000). https://doi.org/10.1023/A:1004654401827
26. J. Souletie, R. Tournier, J. Low Temp. Phys. **1**, 95 (1969). https://doi.org/10.1007/BF00628265